

Numerical evaluation of potential integrals containing higher order hierarchical H(div) Legendre basis functions for parameterized quadrilateral surface cells

Johannesson, Peter; Karlsson, Anders

2011

### Link to publication

Citation for published version (APA):

Johannesson, P., & Karlsson, A. (2011). Numerical evaluation of potential integrals containing higher order hierarchical H(div) Legendre basis functions for parameterized quadrilateral surface cells. (Technical Report LUTEDX/(TEAT-7206)/1-19/(2011); Vol. TEAT-7206). [Publisher information missing].

Total number of authors:

Unless other specific re-use rights are stated the following general rights apply: Copyright and moral rights for the publications made accessible in the public portal are retained by the authors and/or other copyright owners and it is a condition of accessing publications that users recognise and abide by the legal requirements associated with these rights.

• Users may download and print one copy of any publication from the public portal for the purpose of private study

- or research.
- You may not further distribute the material or use it for any profit-making activity or commercial gain
- You may freely distribute the URL identifying the publication in the public portal

Read more about Creative commons licenses: https://creativecommons.org/licenses/

If you believe that this document breaches copyright please contact us providing details, and we will remove access to the work immediately and investigate your claim.

**LUND UNIVERSITY** 

PO Box 117 221 00 Lund +46 46-222 00 00

# Numerical evaluation of potential integrals containing higher order hierarchical H(div) Legendre basis functions for parameterized quadrilateral surface cells

**Peter Johannesson and Anders Karlsson** 

Electromagnetic Theory
Department of Electrical and Information Technology
Lund University
Sweden





Peter Johannesson and Anders Karlsson {Peter.Johannesson,Anders.Karlsson}@eit.lth.se

Department of Electrical and Information Technology Electromagnetic Theory Lund University P.O. Box 118 SE-221 00 Lund Sweden

### Abstract

The singularity cancelation scheme initially introduced by Khayat and Wilton for evaluating singular and near-singular potential integrals with 1/R singularities has in this paper been applied to parameterized quadrilateral cells containing higher order hierarchical  $H(\mathrm{div})$  Legendre basis functions. The singular and near-singular potential integrals treated in this paper appear in the method of moment (MoM). Numerical results are presented for different order numbers of the Legendre polynomials and for quadrilateral cells of different shapes.

### 1 Introduction

EM-modelling of circuite components has received a growing attention during the past ten years. In this area it is crucial to be able to compute circuite parameters of integrated components like transmission lines and other wire based structures, e.g., inductors, baluns and transformers, to a high accuracy. A problem that appears when the MoM is applied to compute the quantities of interest is the "low-frequency catastrophe". This happens when the common rwg basis functions [5] are applied in low-frequency problems. In order to handle this problem one must apply a representation that allows the decomposition of the surface current into a solenoidal part and a nonsolenoidal remainder. One alternative is to use the loop-star basis functions [6] and another is to use large cells including a complex representation that enables the decomposition. A candidate for the second alternative is the higher order hierarchical H(div) basis functions that were introduced in [3]. An advantage of this approach is that the number of degrees of freedom (DOF) can be reduced considerably.

A problem with quasi-static problems is the high demands on the accuracy of the matrix elements and thereby the numerical evaluation of the integrals. This put high demands on the numerical evaluation technique. And due to the properties of the basis functions the technique must also be flexible in order to handle all different cases that appear. The Khayat-Wilton method [4], which is based on the Duffy method [1], fulfills the requirements of accuracy and flexibility. In this paper the Khayat-Wilton method is generalized to handle parameterized quadrilateral cells.

# 2 Preliminaries

The higher order hierarchical basis functions, introduced by Jørgensen et al. [3], yield an efficient way of representing the current density on the surface of the metallization. Since the basis functions are developed for representing currents on quadrilateral surfaces they are well suited for wire shaped structures, like transmission lines. This can be seen by the quadrilateral cell that is illustrated in Figure 1. At the straight parts of the transmission line the quadrilateral cell has a rectangular shape but at corners the more general form is used. This means that the two vectors

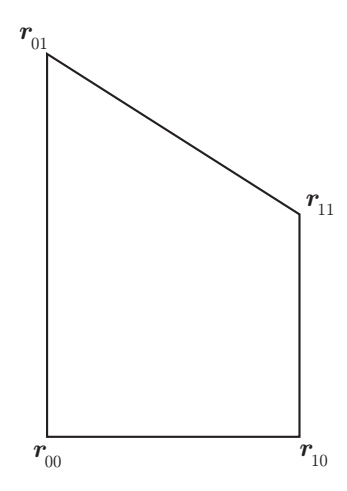


**Figure 1**: A quadrilateral cell.  $r_{ij}$  denotes the coordinates of the vertices.

 $r_{01} - r_{00}$  and  $r_{11} - r_{10}$  are always parallel to each other and orthogonal to the side represented by the vector  $r_{10} - r_{00}$ .

A point in the quadrilateral cell, the domain  $K_{uv}$ , is represented by

$$\mathbf{r}'(u,v) = \mathbf{r}'_c + u\mathbf{r}_u + v\mathbf{r}_v + uv\mathbf{r}_{uv}, \quad -1 \le u, v \le 1, \tag{2.1}$$

where the vectors are

$$\mathbf{r}'_{c} = \frac{1}{4}(\mathbf{r}_{00} + \mathbf{r}_{10} + \mathbf{r}_{01} + \mathbf{r}_{11}), \quad \mathbf{r}_{u} = \frac{1}{4}(-\mathbf{r}_{00} + \mathbf{r}_{10} - \mathbf{r}_{01} + \mathbf{r}_{11}), 
\mathbf{r}_{v} = \frac{1}{4}(-\mathbf{r}_{00} - \mathbf{r}_{10} + \mathbf{r}_{01} + \mathbf{r}_{11}), \quad \mathbf{r}_{uv} = \frac{1}{4}(\mathbf{r}_{00} - \mathbf{r}_{10} - \mathbf{r}_{01} + \mathbf{r}_{11}).$$
(2.2)

The basis functions in [3] are given by

$$\boldsymbol{H}_{mn}^{u}(u,v) = \boldsymbol{a}_{u} \frac{1}{\mathcal{J}_{s}(u,v)} \widetilde{C}_{m} \widetilde{P}_{m}(u) C_{n} P_{n}(v),$$

$$\boldsymbol{H}_{mn}^{v}(u,v) = \boldsymbol{a}_{v} \frac{1}{\mathcal{J}_{s}(u,v)} \widetilde{C}_{m} \widetilde{P}_{m}(v) C_{n} P_{n}(u),$$
(2.3)

where  $a_u$  and  $a_v$  are the contravariant unitary vectors,

$$a_u = \frac{\partial \mathbf{r}'}{\partial u} = \mathbf{r}_u + v \mathbf{r}_{uv}, \quad a_v = \frac{\partial \mathbf{r}'}{\partial v} = \mathbf{r}_v + u \mathbf{r}_{uv},$$
 (2.4)

 $\mathcal{J}_s(u,v) = |\boldsymbol{a}_u \times \boldsymbol{a}_v|$  the surface Jacobian and  $P_n$  the Legendre polynomials. The functions  $\widetilde{P}_m$  are defined as

$$\widetilde{P}_m(x) = \begin{cases} 1 - x, & m = 0, \\ 1 + x, & m = 1, \\ P_m(x) - P_{m-2}(x), & m \ge 2, \end{cases}$$

and the coefficients as

$$\widetilde{C}_m = \begin{cases} \frac{\sqrt{3}}{4}, & m = 0, 1, \\ \frac{1}{2}\sqrt{\frac{(2m-3)(2m+1)}{2m-1}}, & m \ge 2, \end{cases}$$
  $C_n = \sqrt{n+\frac{1}{2}}, n \ge 0.$ 

The integral that represents the cell to cell interaction can be written as linear combinations of the generic integral

$$I_1 = \iiint a(s, t, u, v) P_k(s) P_\ell(t) P_m(u) P_n(v) G(\boldsymbol{r}(s, t), \boldsymbol{r}'(u, v)) \, \mathrm{d}v \, \mathrm{d}u \, \mathrm{d}t \, \mathrm{d}s \quad (2.5)$$

where  $a(s, t, u, v) \in U$  and  $s, t, u, v \in [-1, 1]$ . The set is defined as

$$U = \{ \boldsymbol{a}_s(s,t) \cdot \boldsymbol{a}_u(u,v), \boldsymbol{a}_s(s,t) \cdot \boldsymbol{a}_v(u,v), \boldsymbol{a}_t(s,t) \cdot \boldsymbol{a}_u(u,v), \boldsymbol{a}_t(s,t) \cdot \boldsymbol{a}_v(u,v), 1 \}.$$

The kernel of the integral in (2.5) is weakly singular due to the Green's function,  $G(\mathbf{r}, \mathbf{r}') = \frac{e^{-jk|\mathbf{r}-\mathbf{r}'|}}{4\pi|\mathbf{r}-\mathbf{r}'|}$ . The interaction between a point  $\mathbf{r} \in K_{st}$ , the field point, and the system  $K_{uv}$  is essentially represented by the inner integral

$$I_2(s,t) = \int_{-1}^{1} \int_{-1}^{1} a(s,t,u,v) P_m(u) P_n(v) G(\mathbf{r}(s,t),\mathbf{r}'(u,v)) \, dv \, du.$$
 (2.6)

Due to the singularity, quadrature formulas for functions that can be well approximated by polynomials, e.g., Gauss-Legendre, can not be used to compute the self-couplings. The integral in (2.6) is integrable since the kernel is weakly singular. On contours, efficient techniques for high order accurate integration of many types of singular kernels are readily available, see Section 2 in [2]. On patches, the situation is more involved, even for non-singular kernels, see [7]. This is a vivid research area with important applications.

# 3 Singularity cancelation

# 3.1 Self coupling

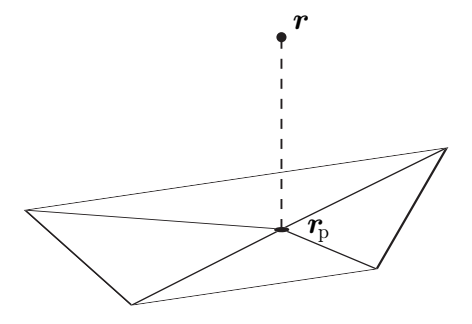


**Figure 2**: Division of the quadrilateral cell into subtriangles in accordance to the Khayat-Wilton method, *i.e.*, the coordinate system is the laboratory system  $K_{xyz}$ .

In order to compute (2.6) in the case of singularities or near-singularities, *i.e.*, when the field point,  $\mathbf{r}$ , is close to the source point,  $\mathbf{r}'$ , the method proposed by Khayat and Wilton [4] is utilized. Applying that technique for a quadrilateral cell

leads to that the cell is divided into four subtriangles, as shown in Figure 2. The four triangles share a common vertex which coincides with the projected field point,  $r_p$ . The integral is thereafter evaluated for each of the subtriangles. This works well as long as the integral is defined in the laboratory system,  $K_{xyz}$ . In the case of parameterized surfaces it is more convenient to evaluate the integral in the local coordinate system. For the integral in (2.6) the local system,  $K_{uv} = \mathbb{R}[-1, 1] \times \mathbb{R}[-1, 1]$ , is represented by a square. Applying the same technique as before conveys four subtriangles in the local system  $K_{uv}$ . This is illustrated in Figure 3. Before

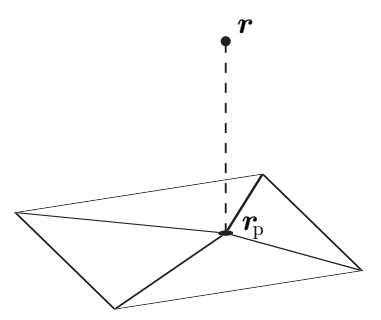


**Figure 3**: Division of the quadrilateral cell into subtriangles in the coordinate system  $K_{uv}$ .

the integration of the subtriangles the coordinates of the projected field point have to be determined. That is, given the coordinates  $(s_0, t_0) \in K_{st}$  find  $(u_0, v_0) \in K_{uv}$ . To do so the coordinate system,  $K_{x^1x^2}$ , that spans the system  $K_{uv}$  in the laboratory system, is introduced. The unit vectors of  $K_{x^1x^2}$  are

$$\hat{oldsymbol{x}}^1 = \hat{oldsymbol{x}}^2 imes \hat{oldsymbol{n}}, \quad \hat{oldsymbol{x}}^2 = rac{oldsymbol{r}_v}{|oldsymbol{r}_v|}$$

where  $\hat{\boldsymbol{n}} = \frac{\boldsymbol{r}_u \times \boldsymbol{r}_v}{|\boldsymbol{r}_u \times \boldsymbol{r}_v|}$ . The coordinates can be found by searching the point (u, v) for which

$$\hat{\boldsymbol{x}}^1 \cdot \boldsymbol{r}(s,t) = \hat{\boldsymbol{x}}^1 \cdot \boldsymbol{r}'(u,v), \quad \hat{\boldsymbol{x}}^2 \cdot \boldsymbol{r}(s,t) = \hat{\boldsymbol{x}}^2 \cdot \boldsymbol{r}'(u,v)$$
(3.1)

is fulfilled.

Let  $\mathbf{r}_u = x_u^1 \hat{\mathbf{x}}^1 + x_u^2 \hat{\mathbf{x}}^2$ , in (2.2), with corresponding expressions for  $\mathbf{r}_v$ ,  $\mathbf{r}_{uv}$ . Then the coordinates are given by

$$ux_u^1 + vx_v^1 + uvx_{uv}^1 = f(s,t), \quad uy_u^2 + vy_v^2 + uvy_{uv}^2 = g(s,t)$$
(3.2)

where

$$f(s,t) = \hat{\boldsymbol{x}}^1 \cdot (\boldsymbol{r}(s,t) - \boldsymbol{r}'_c),$$
  $g(s,t) = \hat{\boldsymbol{x}}^2 \cdot (\boldsymbol{r}(s,t) - \boldsymbol{r}'_c).$ 

Combining the two equations in (3.2) yields

$$\alpha_u u^2 + \beta_u u - \gamma_u = 0, \qquad \alpha_v v^2 + \beta_v v - \gamma_v = 0$$

where

$$\alpha_{u} = x_{uv}^{1} x_{u}^{2} - x_{u}^{1} x_{uv}^{2}, \qquad \alpha_{v} = x_{uv}^{1} x_{v}^{2} - x_{v}^{1} x_{uv}^{2}, 
\beta_{u} = x_{v}^{1} x_{u}^{2} - x_{u}^{1} x_{v}^{2} + f x_{uv}^{2} - g x_{uv}^{1}, \qquad \beta_{v} = x_{u}^{1} x_{v}^{2} - x_{v}^{1} x_{u}^{2} + f x_{uv}^{2} - g x_{uv}^{1}, 
\gamma_{u} = -f x_{v}^{2} + g x_{v}^{1}, \qquad \gamma_{v} = -f x_{u}^{2} + g x_{u}^{1}.$$

The solutions to the two second order equations are

$$\begin{aligned} \alpha_u &= 0, \beta_u \neq 0, & u_0 &= \gamma_u/\beta_u, \\ \alpha_u &\neq 0, \beta_u &= 0, & u_0 &= \pm \sqrt{\gamma_u/\alpha_u}, \\ \alpha_u &\neq 0, \beta_u &\neq 0, & u_0 &= -\frac{\beta_u}{2\alpha_u} \pm \sqrt{\left(\frac{\beta_u}{2\alpha_u}\right)^2 + \frac{\gamma_u}{\alpha_u}}, \\ \alpha_v &= 0, \beta_v &\neq 0, & v_0 &= \gamma_v/\beta_v, \\ \alpha_v &\neq 0, \beta_v &= 0, & v_0 &= \pm \sqrt{\gamma_v/\alpha_v}, \\ \alpha_v &\neq 0, \beta_v &\neq 0, & v_0 &= -\frac{\beta_v}{2\alpha_v} \pm \sqrt{\left(\frac{\beta_v}{2\alpha_v}\right)^2 + \frac{\gamma_v}{\alpha_v}}. \end{aligned}$$

For the quadrilateral cell (see Figure 1)  $\mathbf{r}_{uv}$  and  $\mathbf{r}_v$  are always parallel. This conveys that  $\alpha_v = x_{uv}^1 x_v^2 - x_v^1 x_{uv}^2 = \mathbf{r}_{uv} \times \mathbf{r}_v = \mathbf{0}$ . The solution for  $v_0$  is thus given by  $v_0 = \gamma_v/\beta_v$ ,  $\beta_v \neq 0$ . The case when  $\beta_v = 0$  corresponds to the case when v is ambiguous which means that there is an infinite number of solutions. This happens when  $\mathbf{r}_v + u\mathbf{r}_{uv} = \mathbf{0}$ , in the expression  $\mathbf{r} = \mathbf{r}_c + u\mathbf{r}_u + v\mathbf{r}_v + uv\mathbf{r}_{uv}$ , and corresponds to the u-value  $u_a = -\frac{\mathbf{r}_v \cdot \mathbf{r}_v}{\mathbf{r}_v \cdot \mathbf{r}_{uv}}$ . Since the solutions to (3.2) are  $(u_0, v_0)$  and  $(u_a, v_0)$ , the correct solution is achieved by simple comparison. If the field point  $\mathbf{r}(s,t)$  coincides with  $\mathbf{r}_a$  no unambiguous solution exists which means that the point can not be used as a quadrature point. A simple displacement,  $\mathbf{r}(s,t) := \mathbf{r}(s,t) + \Delta \mathbf{r}$ , is an easy way to solve the problem. The displacement  $\Delta \mathbf{r}$  has to be small in comparison to the distance between the two closest quadrature points.

The relation for  $\alpha_u$  and  $\beta_u$  can be written as

$$\alpha_u = x_{uv}^1 x_u^2 - x_u^1 x_{uv}^2 = (\boldsymbol{r}_{uv} \times \boldsymbol{r}_u) \cdot \hat{\boldsymbol{n}},$$
  
$$\beta_u = x_v^1 x_u^2 - x_u^1 x_v^2 + f x_{uv}^2 - g x_{uv}^1 = (\boldsymbol{r}_v \times \boldsymbol{r}_u) \cdot \hat{\boldsymbol{n}} + ((\boldsymbol{r}(s,t) - \boldsymbol{r}_c') \times \boldsymbol{r}_{uv}) \cdot \hat{\boldsymbol{n}}.$$

Since  $\mathbf{r}_{uv} = \mathbf{0}$  in the case of a rectangular quadrilateral we find that  $\alpha_u = 0$  and  $\beta_u \neq 0$ . For the more general cell structures, as in Figure 1,  $\mathbf{r}_{uv} \times \mathbf{r}_u \neq \mathbf{0}$  and  $\mathbf{r}_{uv} \cdot \mathbf{r}_u \neq \mathbf{0}$  which conveys  $\alpha_u \neq 0$ . Thus, the case when  $\alpha_u = 0$  and  $\beta_u = 0$  does not occur. The solutions to (3.2) are given by

$$\alpha_{u} = 0, \beta_{u} \neq 0, \qquad u_{0} = \gamma_{u}/\beta_{u},$$

$$\alpha_{u} \neq 0, \beta_{u} = 0, \qquad u_{0} = \pm \sqrt{\gamma_{u}/\alpha_{u}},$$

$$\alpha_{u} \neq 0, \beta_{u} \neq 0, \qquad u_{0} = -\frac{\beta_{u}}{2\alpha_{u}} \pm \sqrt{\left(\frac{\beta_{u}}{2\alpha_{u}}\right)^{2} + \frac{\gamma_{u}}{\alpha_{u}}},$$

$$\beta_{v} \neq 0, \qquad v_{0} = \gamma_{v}/\beta_{v}.$$

The domain  $K_{uv}$  is divided into subtriangles,  $T_i$ , by introducing a line,  $L_j$ , between the point  $\mathbf{r}_p = (u_0, v_0)$  and the four vertices,  $\mathbf{r}_{ij}$ , as illustrated in Figure 4. The four lines are represented by

$$L_1: u_1(v) = k_1 v + \ell_1, v_1(u) = p_1 u + q_1,$$

$$L_2: u_2(v) = k_2 v + \ell_2, v_2(u) = p_2 u + q_2,$$

$$L_3: u_3(v) = k_3 v + \ell_3, v_3(u) = p_3 u + q_3,$$

$$L_4: u_4(v) = k_4 v + \ell_4, v_4(u) = p_4 u + q_4,$$

where the coefficients are

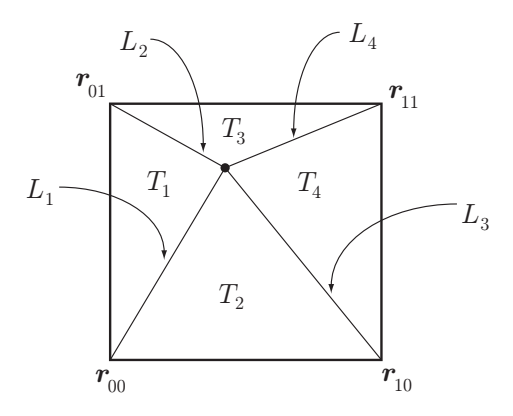


**Figure 4**: The quadrilateral cell in the  $K_{uv}$  domain. The four triangles  $T_i$  are separated by the lines  $L_j$ .

$$k_{1} = \frac{-1 - u_{0}}{-1 - v_{0}}, \quad \ell_{1} = -1 + k_{1},$$

$$k_{2} = \frac{-1 - u_{0}}{1 - v_{0}}, \quad \ell_{2} = -1 - k_{2},$$

$$k_{3} = \frac{1 - u_{0}}{-1 - v_{0}}, \quad \ell_{3} = 1 + k_{3},$$

$$k_{4} = \frac{1 - u_{0}}{1 - v_{0}}, \quad \ell_{4} = -1 - k_{4},$$

$$p_{i} = \frac{1}{k_{i}}, \quad q_{i} = -\frac{\ell_{i}}{k_{i}}, \quad i = \{1, 2, 3, 4\}.$$

The integral in (2.6) is divided into four integrals, one for each triangle,  $T_i$ ,

$$T_{1}: \int_{-1}^{u_{0}} du \int_{v_{1}(u)}^{v_{2}(u)} dv \frac{f_{mn}(s,t,u,v)}{|\boldsymbol{r}(s,t)-\boldsymbol{r}'(u,v)|}, \qquad T_{2}: \int_{-1}^{v_{0}} dv \int_{u_{1}(v)}^{u_{3}(v)} du \frac{f_{mn}(s,t,u,v)}{|\boldsymbol{r}(s,t)-\boldsymbol{r}'(u,v)|},$$

$$T_{3}: \int_{v_{0}}^{1} dv \int_{u_{2}(v)}^{u_{4}(v)} du \frac{f_{mn}(s,t,u,v)}{|\boldsymbol{r}(s,t)-\boldsymbol{r}'(u,v)|}, \qquad T_{4}: \int_{u_{0}}^{1} du \int_{v_{3}(u)}^{v_{4}(u)} dv \frac{f_{mn}(s,t,u,v)}{|\boldsymbol{r}(s,t)-\boldsymbol{r}'(u,v)|},$$

where

$$f_{mn}(s, t, u, v) = \frac{1}{4\pi} a(s, t, u, v) P_m(u) P_n(v) e^{-jk|r(s,t)-r'(u,v)|}$$

In order to eliminate the singularity a proper variable substitution in the inner integral is needed. This is achieved by first inserting (2.1) into  $|\mathbf{r} - \mathbf{r}'|$  in the local system,  $K_{uv}$ . For the triangles  $T_1$  and  $T_4$  this gives

$$|\boldsymbol{r} - \boldsymbol{r}'| = a_v(u)\widetilde{R}_v(u,v)$$

where

$$\widetilde{R}_{v}(u,v) = \sqrt{v^{2} + b_{v}(u)v + c_{v}(u)}, \quad a_{v}^{2}(u) = u^{2} |\boldsymbol{r}_{uv}|^{2} + 2u\boldsymbol{r}_{v} \cdot \boldsymbol{r}_{uv} + |\boldsymbol{r}_{v}|^{2},$$

$$b_{v}(u) = 2(u^{2}\boldsymbol{r}_{u} \cdot \boldsymbol{r}_{uv} - u\boldsymbol{r} \cdot \boldsymbol{r}_{uv} + u\boldsymbol{r}'_{c} \cdot \boldsymbol{r}_{uv} + u\boldsymbol{r}_{u} \cdot \boldsymbol{r}_{v} - \boldsymbol{r} \cdot \boldsymbol{r}_{v} + \boldsymbol{r}'_{c} \cdot \boldsymbol{r}_{v})/a_{v}^{2}(u),$$

$$c_{v}(u) = (u^{2} |\boldsymbol{r}_{u}|^{2} - 2u\boldsymbol{r} \cdot \boldsymbol{r}_{u} + 2u\boldsymbol{r}'_{c} \cdot \boldsymbol{r}_{u} + |\boldsymbol{r}|^{2} - 2\boldsymbol{r} \cdot \boldsymbol{r}'_{c} + |\boldsymbol{r}'_{c}|^{2})/a_{v}^{2}(u).$$

and for the triangles  $T_2$  and  $T_3$  we get

$$|\boldsymbol{r} - \boldsymbol{r}'| = a_u(v)\widetilde{R}_u(u,v)$$

where

$$\widetilde{R}_{u}(u,v) = \sqrt{u^{2} + b_{u}(v)u + c_{u}(v)}, \quad a_{u}^{2}(v) = v^{2} |\boldsymbol{r}_{uv}|^{2} + 2v\boldsymbol{r}_{u} \cdot \boldsymbol{r}_{uv} + |\boldsymbol{r}_{u}|^{2},$$

$$b_{u}(v) = 2(v^{2}\boldsymbol{r}_{v} \cdot \boldsymbol{r}_{uv} - v\boldsymbol{r} \cdot \boldsymbol{r}_{uv} + v\boldsymbol{r}'_{c} \cdot \boldsymbol{r}_{uv} + v\boldsymbol{r}_{u} \cdot \boldsymbol{r}_{v} - \boldsymbol{r} \cdot \boldsymbol{r}_{u} + \boldsymbol{r}'_{c} \cdot \boldsymbol{r}_{u})/a_{u}^{2}(v),$$

$$c_{u}(v) = (v^{2} |\boldsymbol{r}_{v}|^{2} - 2v\boldsymbol{r} \cdot \boldsymbol{r}_{v} + 2v\boldsymbol{r}'_{c} \cdot \boldsymbol{r}_{v} + |\boldsymbol{r}|^{2} - 2\boldsymbol{r} \cdot \boldsymbol{r}'_{c} + |\boldsymbol{r}'_{c}|^{2})/a_{u}^{2}(v),$$

By thereafter choosing  $dw_v = \frac{dv}{\tilde{R}_v}$  and  $dw_u = \frac{du}{\tilde{R}_u}$  with the primitive functions

$$w_u(u,v) = \frac{1}{2} \ln \left( \frac{\widetilde{R}_u(u,v) + u + \frac{1}{2}b_u(v)}{\widetilde{R}_u(u,v) - u - \frac{1}{2}b_u(v)} \right),$$

$$w_v(u,v) = \frac{1}{2} \ln \left( \frac{\widetilde{R}_v(u,v) + v + \frac{1}{2}b_v(u)}{\widetilde{R}_v(u,v) - v - \frac{1}{2}b_v(u)} \right)$$

the singularity is eliminated and the four integrals become

$$T_{1}: \int_{-1}^{u_{0}} du \int_{w_{v}(u,v_{1}(u))}^{w_{v}(u,v_{2}(u))} dw_{v} \frac{f_{mn}(s,t,u,v(w_{v}))}{a_{v}(u)},$$

$$T_{2}: \int_{-1}^{v_{0}} dv \int_{w_{u}(u_{1}(v),v)}^{w_{u}(u_{3}(v),v)} dw_{u} \frac{f_{mn}(s,t,u(w_{u}),v)}{a_{u}(v)},$$

$$T_{3}: \int_{v_{0}}^{1} dv \int_{w_{u}(u_{2}(v),v)}^{w_{u}(u_{4}(v),v)} dw_{u} \frac{f_{mn}(s,t,u(w_{u}),v)}{a_{u}(v)},$$

$$T_{4}: \int_{u_{0}}^{1} du \int_{w_{v}(u,v_{3}(u))}^{w_{v}(u,v_{3}(u))} dw_{v} \frac{f_{mn}(s,t,u,v(w_{v}))}{a_{v}(u)}.$$

$$(3.3)$$

To find expressions for the inverse functions,  $u(w_u)$  and  $v(w_v)$ , the alternative representation of the primitive functions

$$w_u(u) = \sinh^{-1}\left(\frac{u + b_u/2}{\sqrt{c_u - b_u^2/4}}\right), \qquad w_v(v) = \sinh^{-1}\left(\frac{v + b_v/2}{\sqrt{c_v - b_v^2/4}}\right)$$

is applied to achieve

$$u(w_u) = \sqrt{c_u - \frac{b_u^2}{4}} \sinh(w_u) - \frac{b_u}{2}, \qquad v(w_v) = \sqrt{c_v - \frac{b_v^2}{4}} \sinh(w_v) - \frac{b_v}{2}.$$

**Example 3.1.** Consider the quadrilateral in Figure 5. The field point, r, is chosen to be in the first quadrant of the quadrilateral cell, as is illustrated in the left figure in Figure 5 where the field point is marked with a cross. To illustrate how the singularity cancelation works we choose the triangular region  $T_2$ , see the right figure in Figure 5, and maps it on the region  $T'_2$  in the  $K_{vw}$  domain. This is illustrated in Figure 6. Due to the limitations in the Gauss-Legendre method stair-case

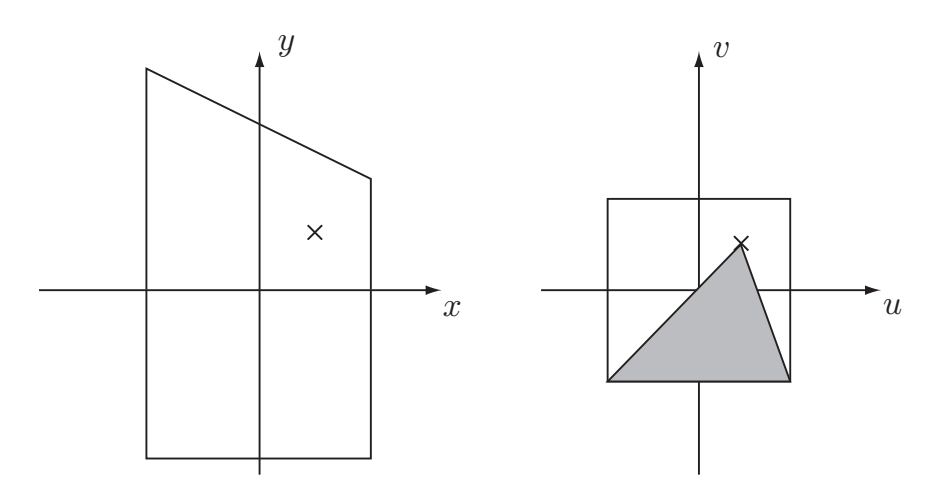


**Figure 5**: The quadrilateral surface and the  $K_{uv}$  domain with the singular point  $(u_0, v_0)$  in Example 3.1.

approximations are used to represent the contour of the  $T_2'$  region. This implies that the shape of the region  $T_2'$  affects the accuracy of the quadrature method. The stair-case approximation works well as long as the contour does not contain lines of sharp curvature and the corners not are too sharp. Since the  $T_2'$  region is very close to a parallelogram, where the contour consist of lines that are almost straight, it is expected that the shape only will have a minor impact on the accuracy of the quadrature method. This means that the accuracy essentially is determined by the integrand in (2.6). The integrand is a polynomial in u and v times an exponential function. In the low frequency case, when the cell size is much smaller than the wavelength, the exponential function is almost constant and the numerical integration becomes quite straightforward, especially in the case of zeroth order

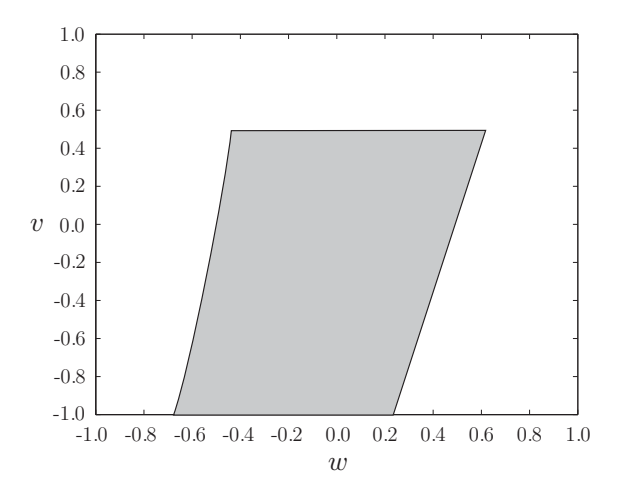


**Figure 6**: The integration region in the  $K_{vw}$  domain. The  $T'_2$  region is the mapping of the  $T_2$  triangle in Figure 5.

polynomials. In that case the integrand is almost constant which means that only one or two quadrature points, in each direction, are necessary in order to achieve a sufficient accuracy.

### 3.2 Mutual interaction

The emphasis so far, in the analysis, has been to the case when the projection of the field point is in the domain of integration, *i.e.*,  $r_p \in K_{uv}$ . To be able to handle the case when  $r_p \notin K_{uv}$  the integrals in (3.3) can not be used directly. The reason is

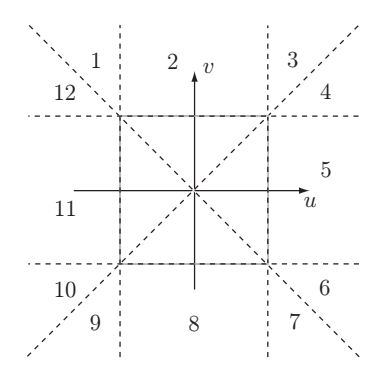


Figure 7: Twelve different regions where the near-singular point can be.

that the argument of the Legendre polynomials is outside  $K_{uv}$  which leads to several bad features, e.g., the orthogonality is lost and the  $P_n$  do not fulfill  $P_n \in [-1,1]$ . Since  $P_n$  might loose its polynomial behavior in the domains  $w_u$  and  $w_v$  the rapid variation of the function, for the larger values of the order number, outside the  $K_{uv}$  domain can affect the convergence of the Gauss-Legendre algorithm in a negative

way. In order to handle the case when the projection of the field point is outside the quadrilateral cell special rules have to be developed.

Now focus on Figure 7. Here the domain outside  $K_{uv}$  has been divided into twelve regions. If region two and three are considered, as special cases, we find that when the field point is in region two the three integrals that correspond to the triangles  $T_1, T_2$  and  $T_4$  are applied and when the field point is in region three the two integrals that correspond to the triangles  $T_1$  and  $T_2$  are applied. This is illustrated in Figure 8. The two cases can be seen as representations of the different cases of

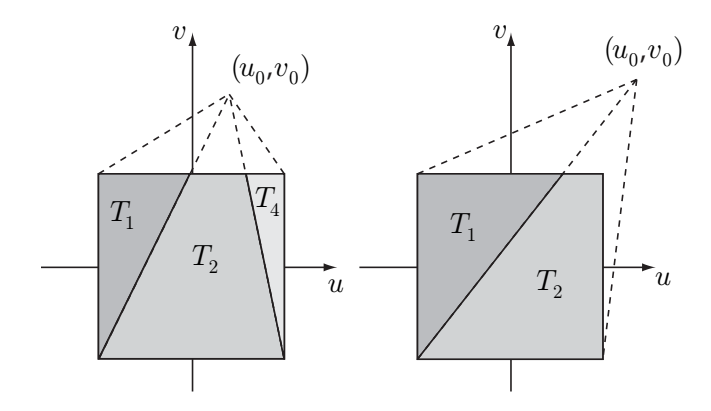


Figure 8: Two of the basic cases of integration.

integration that exist. The partial integrals in region two are given by

$$T_{1}: \int_{-1}^{u_{1}(1)} du \int_{v_{1}(u)}^{1} dv \frac{f_{mn}(s,t,u,v)}{|\boldsymbol{r}(s,t)-\boldsymbol{r}'(u,v)|},$$

$$T_{2}: \int_{-1}^{1} dv \int_{u_{1}(v)}^{u_{3}(v)} du \frac{f_{mn}(s,t,u,v)}{|\boldsymbol{r}(s,t)-\boldsymbol{r}'(u,v)|},$$

$$T_{4}: \int_{u_{3}(1)}^{1} du \int_{v_{3}(u)}^{1} dv \frac{f_{mn}(s,t,u,v)}{|\boldsymbol{r}(s,t)-\boldsymbol{r}'(u,v)|}$$

and in region three by

$$T_1: \int_{-1}^{u_1(1)} du \int_{v_1(u)}^{1} dv \frac{f_{mn}(s,t,u,v)}{|\boldsymbol{r}(s,t)-\boldsymbol{r}'(u,v)|}, \quad T_2: \int_{-1}^{1} dv \int_{u_1(v)}^{1} du \frac{f_{mn}(s,t,u,v)}{|\boldsymbol{r}(s,t)-\boldsymbol{r}'(u,v)|}.$$

The integral expressions for the other cases are achieved in a similar way.

**Example 3.2.** Consider the quadrilateral cell in Figure 9. In order to illustrate how the domain of integration is mapped in the case of mutual interaction the field point

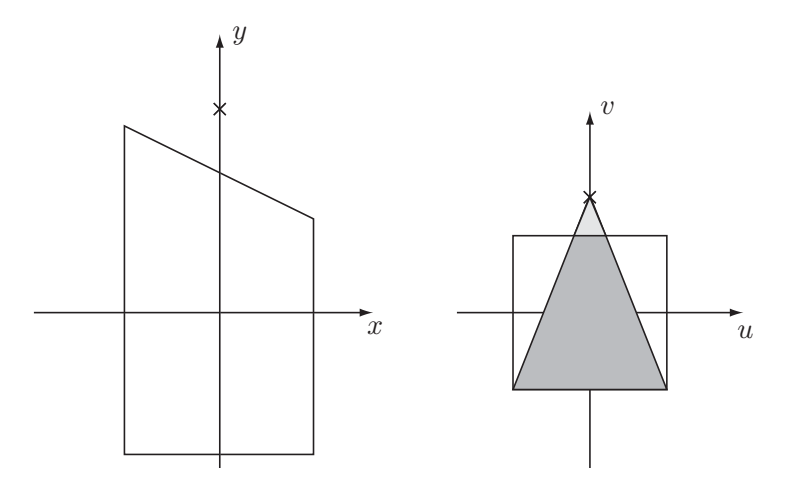


**Figure 9**: The quadrilateral surface and the  $K_{uv}$  domain with the singular point at  $(u_0, v_0)$  in Example 3.2. The cross in the left figure indicates the singular point in the  $K_{xyz}$  domain. The region of integration is the darker shaded region.

has been chosen to be on the positive y-axis, outside the quadrilateral cell. This is marked with a cross in the left figure in Figure 9. Once again the triangular domain,  $T_2$ , is chosen to illustrate the mapping. As can be seen in the right figure in Figure 9 the triangular region is divided into two sub-regions. This is due to the properties of the Legendre polynomials. This means that only the part of the triangle that coincide with the  $K_{uv}$  domain is mapped to the  $K_{vw}$  domain. This region,  $T'_2$ , is the darker shaded region and is illustrated in Figure 10. The darker shaded region

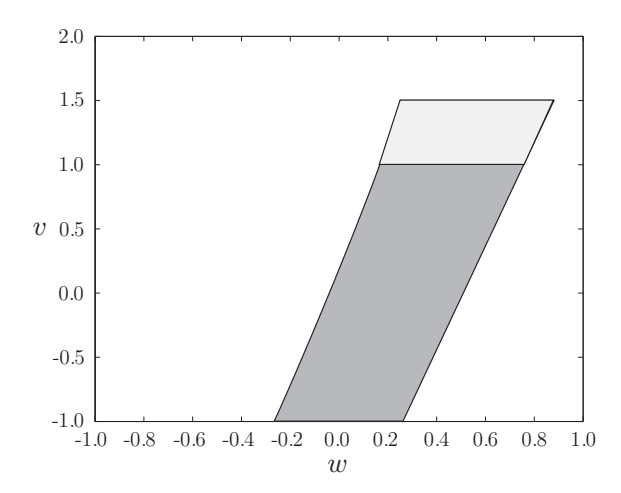


**Figure 10**: The integration region in the (v, w) system. The  $T'_2$  region is the mapping of the  $T_2$  triangle in Figure 9. It is only necessary to integrate over the darker shaded region.

corresponds to the domain of integration whereas the remaining part corresponds to the region outside the  $K_{uv}$  domain and does not belong to the domain of integration.

Note that the limits of the v-variable, in the  $K_{vw}$  domain, are  $v \in [-1, 1]$ . Since the  $T'_2$  region is very close to a parallelogram the shape of the region will not significantly reduce the accuracy of the quadrature method leading to that the accuracy of the method is essentially limited by the integrand.

**Example 3.3.** In the previous two examples the chosen position of the field point resulted in an partial integration region, the  $T'_2$ -region, with a shape close to a parallelogram. This form is suitable for the Gauss-Legendre quadrature rule since the stair-case approximation of the contour of the  $T'_2$ -region only has a minor impact on the accuracy of the quadrature method. By moving the field point closer to one of the corners, illustrated in the left figure in Figure 11, the dark shaded sub-region, in the right figure in Figure 11, becomes more complex. The mapping of the dark

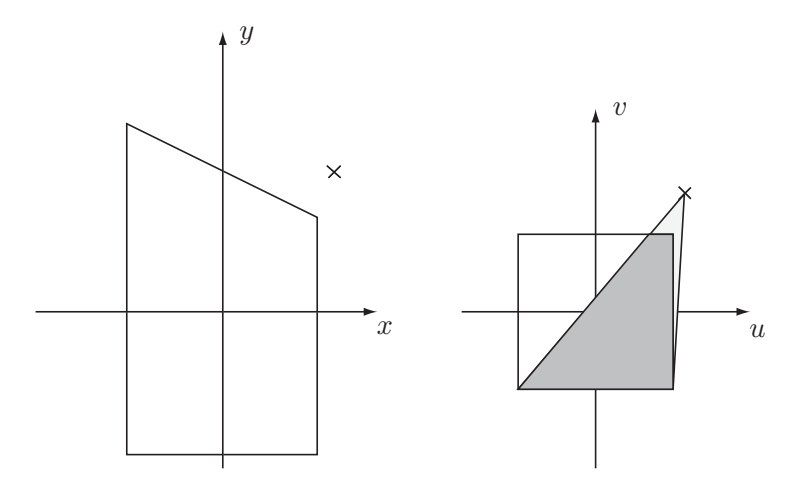


**Figure 11**: The quadrilateral cell and the  $K_{uv}$  domain with the singular point at  $(u_0, v_0)$  in Example 3.3. The cross in the left figure indicates the singular point in the  $K_{xyz}$  domain. The domain of integration is the darker shaded region.

shaded region, in the  $K_{uv}$  domain, is illustrated in Figure 12 where the mapping corresponds to the dark shaded region, in the  $K_{vw}$  domain, the  $T'_2$  region. The light shaded region in Figure 12 corresponds to the light shaded region outside the  $K_{uv}$  domain. As can be seen the  $T'_2$  region no longer has the shape of a parallelogram. The almost straight lines, on the left and right side of the  $T'_2$  region, have been replaced by curved lines where the line on the right side has the largest curvature. Due to the limitations in the stair-case approximation the introduction of the curved lines lead to a degradation of the accuracy of the quadrature method. This means that it requires a larger number of quadrature points to achieve the same accuracy which leads to a slower convergence rate.

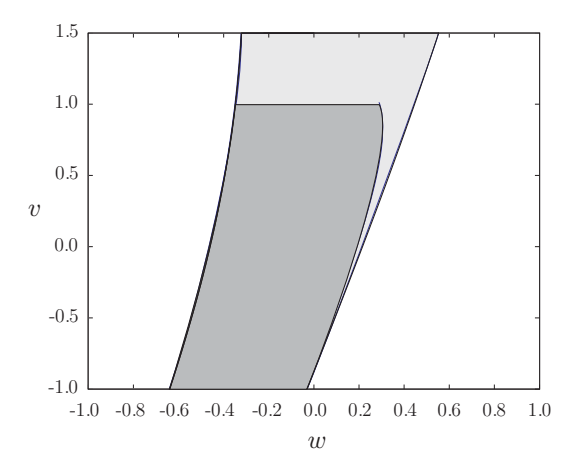


**Figure 12**: The integration region in the  $K_{vw}$  domain. The dark shaded region is the mapping of the domain of integration in Figure 11 and the light shaded region is the mapping of the light shaded sub-region.

**Example 3.4.** By moving the field point even closer to the top right corner, compared to the position of the field point in Example 3.3, yields an integration region that is more severe than the one presented in Example 3.3. The quadrilateral cell and the field point is illustrated in Figure 13 and the resulting integration region  $T_2'$  is illustrated in Figure 14. And as in the previous examples it is only the dark shaded

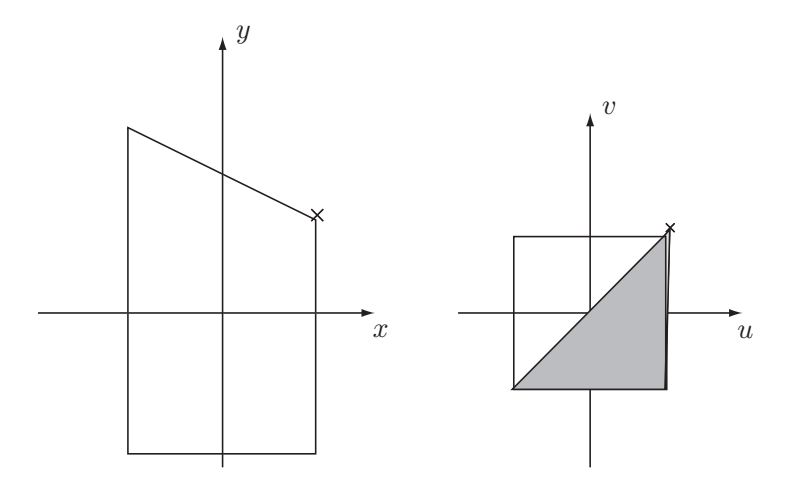


**Figure 13**: The quadrilateral cell and the  $K_{uv}$  domain with the singular point at  $(u_0, v_0)$  in Example 3.4. The cross in the left figure indicates the singular point in the  $K_{xyz}$  domain. The domain of integration is the darker shaded region.

region that represents the integration region. By studying the  $T'_2$  region in the  $K_{vw}$  domain in Figure 14 it is found that the upper right corner has been replaced by a curved line for which the curvature is rather high. This part becomes the bottleneck during the numerical quadrature, due to the stair-case approximation, which leads

to a significant reduction of the convergence rate.

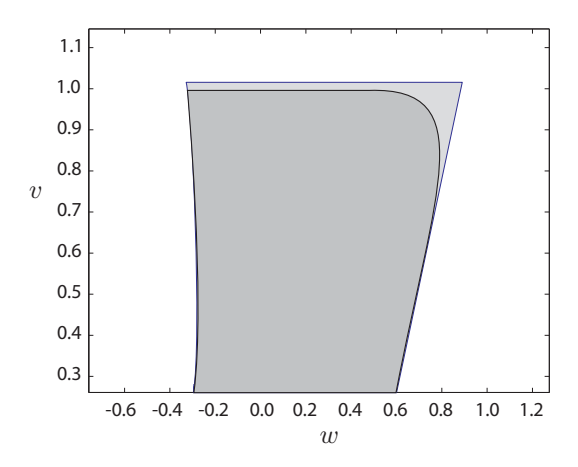


**Figure 14**: The integration region in the  $K_{vw}$  domain. The dark shaded region is the mapping of the domain of integration in Figure 13 and the light shaded region is the mapping of the light shaded sub-region.

### 4 Results

The integral  $I_2$ , in (2.6), has been computed for three examples including two different cell shapes: a quadrilateral and a rectangular cell. The coordinates of the vertices for the quadrilateral cell are  $\mathbf{r}_{00} = (-1, -1.5, 0)$ ,  $\mathbf{r}_{01} = (-1, 2, 0)$ ,  $\mathbf{r}_{10} = (1, -1.5, 0)$ ,  $\mathbf{r}_{11} = (1, 1, 0)$  and the coordinates for the rectangular cell are  $\mathbf{r}_{00} = (-1, -1.5, 0)$ ,  $\mathbf{r}_{01} = (-1, 1.5, 0)$ ,  $\mathbf{r}_{10} = (1, -1.5, 0)$  and  $\mathbf{r}_{11} = (1, 1.5, 0)$ . In order to measure the accuracy of the method a relative error is introduces. It is defined as

$$\eta = \frac{I_2 - I_{2,N}}{|I_2|}$$

where  $I_2$  is the reference value, computed via the software Mathematica, and  $I_{2,N}$  is computed via the method presented in this paper. N represents the number of quadrature points.

The first example addresses the impact of the cell shapes on the accuracy. The convergence rate for the quadrilateral and the rectangular cell is compared for the case when the field point is placed at  $\mathbf{r} = (0,0,0)$ . The results are presented in Figure 15 and Figure 16. For the rectangular cell the case m = n = 1 is missing. The reason is that the integral vanishes for this case and has therefore not been included.

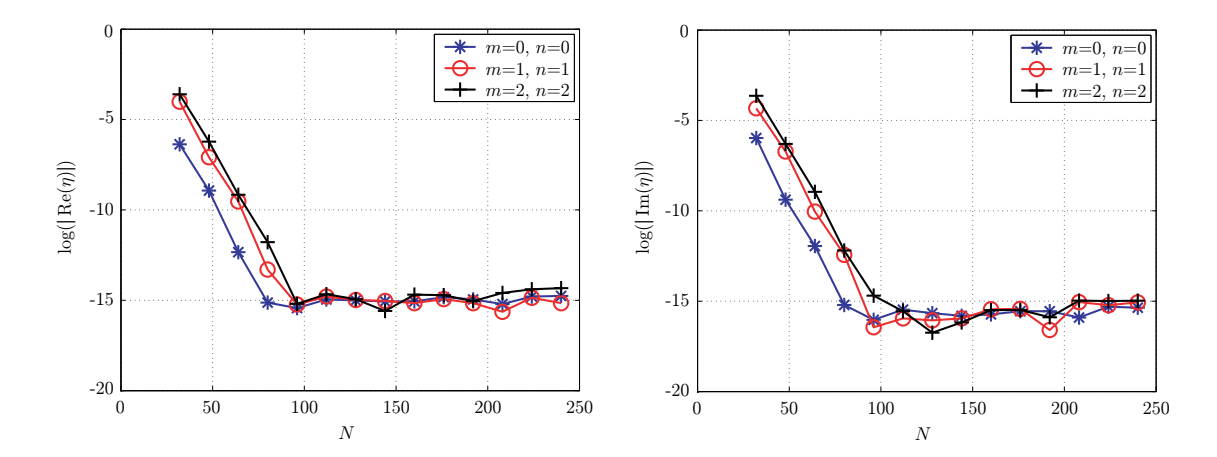


**Figure 15**: The relative error at  $\mathbf{r} = (0, 0, 0)$  in the case of a quadrilateral cell as a function of the number of quadrature points. The results in the left (right) figure are the real (imaginary) part of the relative error for the quadrilateral cell.

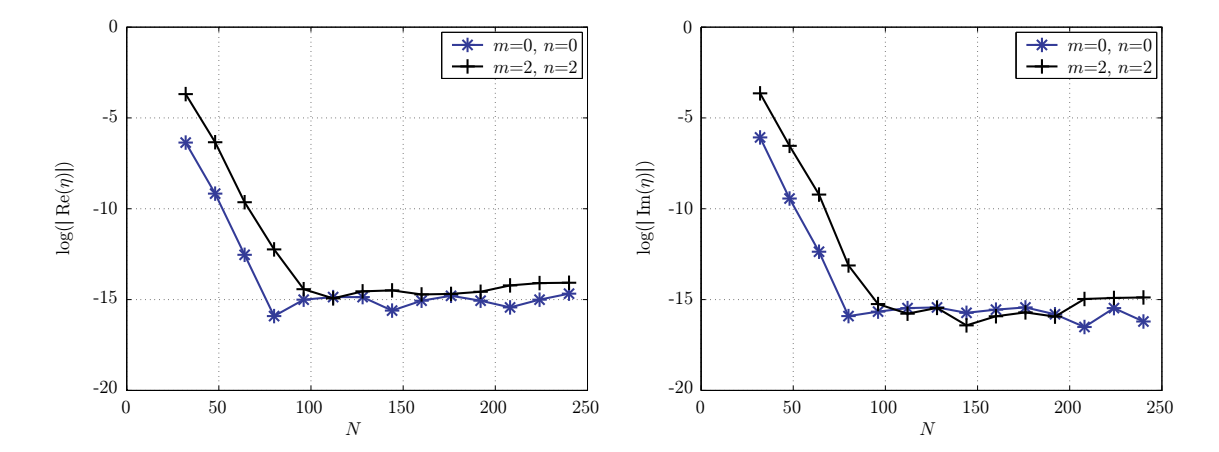


**Figure 16**: The relative error at  $\mathbf{r} = (0,0,0)$  in the case of a rectangular cell as a function of the number of quadrature points. The results in the left (right) figure are the real (imaginary) part of the relative error for the rectangular cell.

In the second example the field point is placed at the position  $\mathbf{r} = (0, 0, d)$ , d > 0 (see Figure 2). The convergence rate is thereafter examined for two different values on d. The results are presented in Figure 17 and Figure 18.

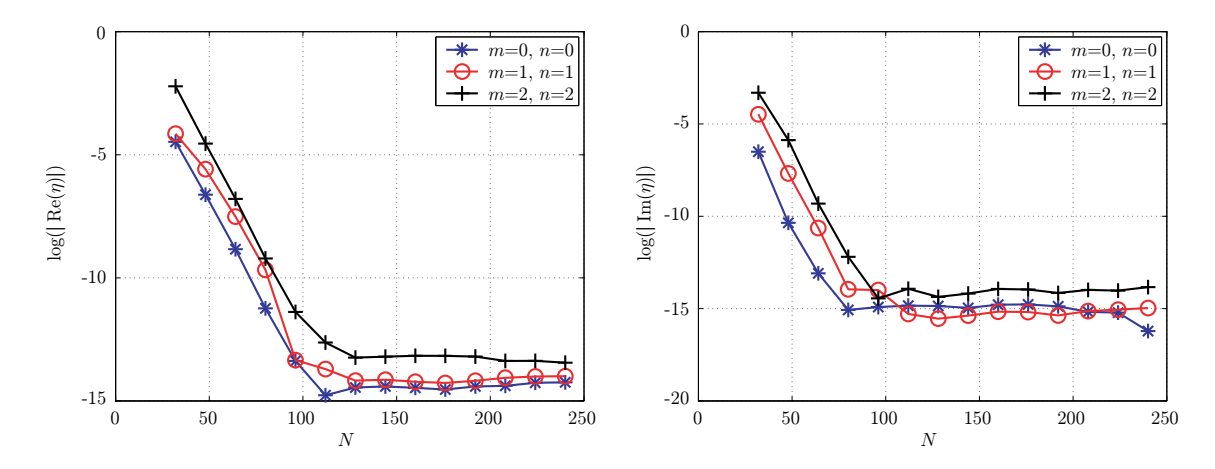


**Figure 17**: The relative error in the case of a quadrilateral cell. The left (right) figure represents the real (imaginary) part of the relative error at  $\mathbf{r} = (0, 0, 1)$ .

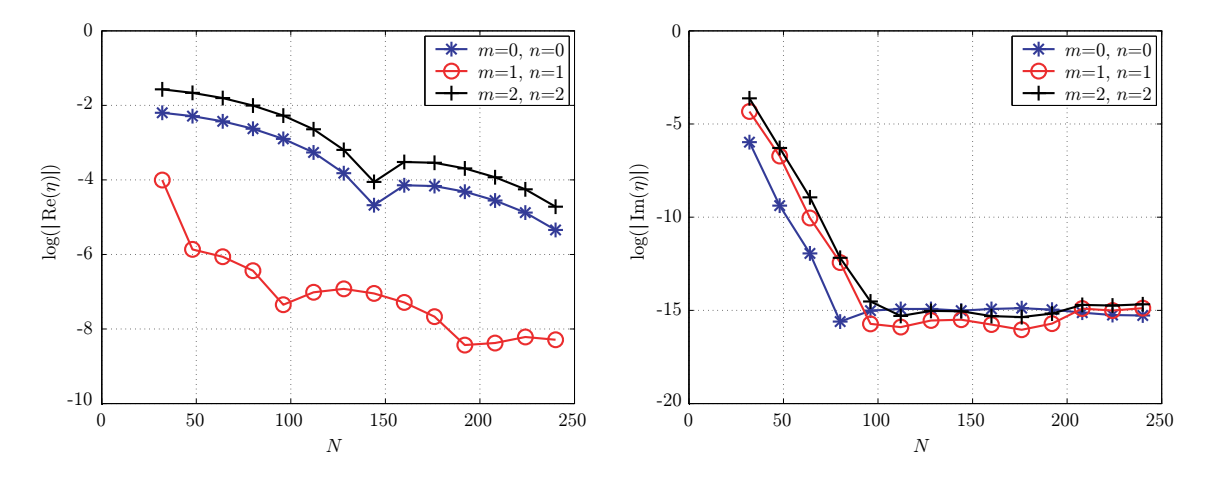
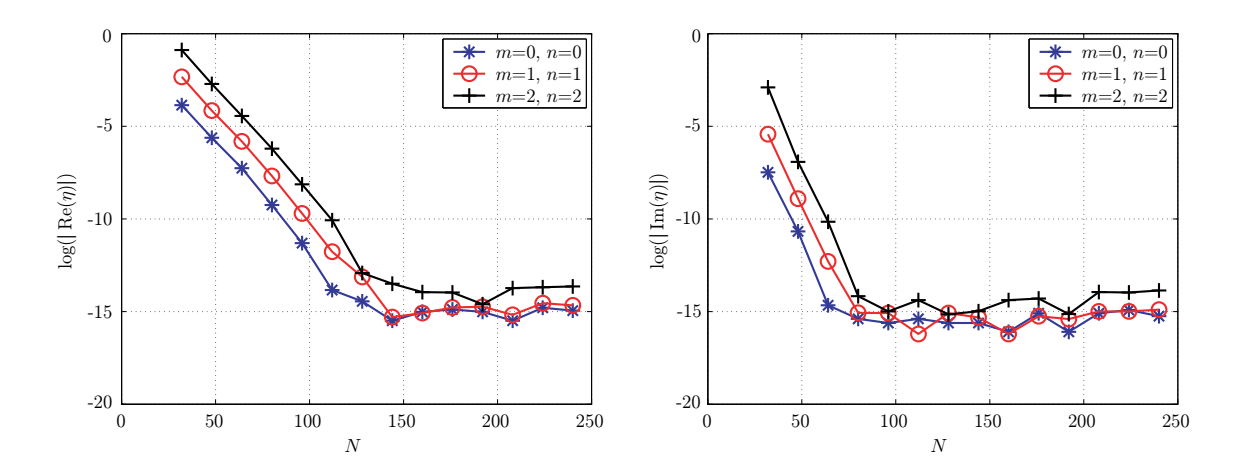
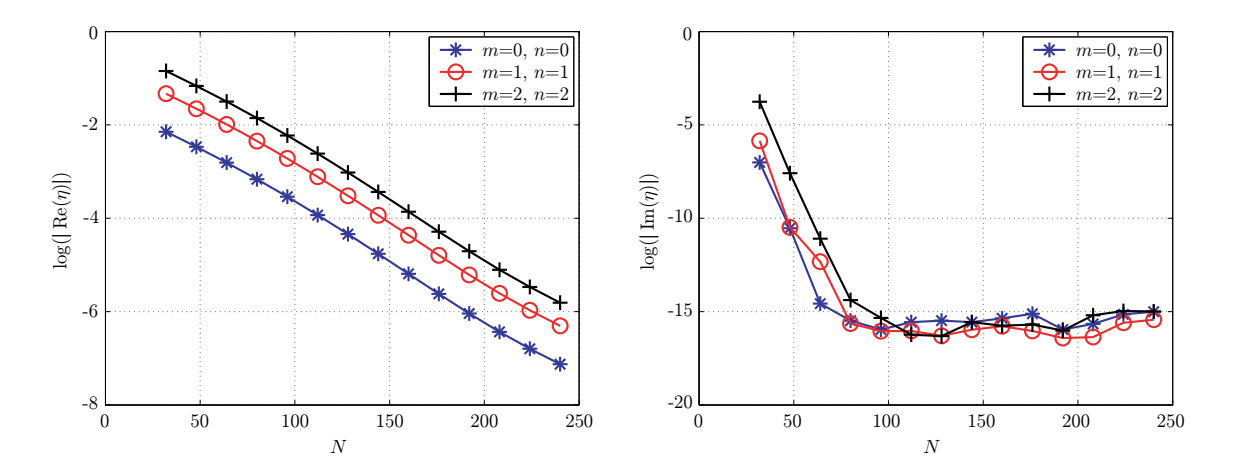


Figure 18: The relative error in the case of a quadrilateral cell. The left (right) figure represents the real (imaginary) part of the relative error at  $\mathbf{r} = (0, 0, 0.01)$ .

In the third example the field point is placed at a position outside the domain of integration but on the same plane, i.e.,  $\mathbf{r} = \{\mathbf{r}_p : \mathbf{r}_p \notin K_{uv}\}$ . The convergence rate is thereafter investigated for two different positions in this domain: one position on a distance from the boundary of the cell and one position at the vicinity of the boundary. The results are presented in Figure 19 and Figure 20.



**Figure 19**: The relative error in the case of a quadrilateral cell. The left (right) figure represents the real (imaginary) part of the relative error at  $\mathbf{r} = (1.2, 1.5, 0)$ .



**Figure 20**: The relative error in the case of a quadrilateral cell. The left (right) figure represents the real (imaginary) part of the relative error at  $\mathbf{r} = (1.01, 1.02, 0)$ .

## 5 Conclusions

The Khayat-Wilton method has in this paper been applied to parameterized quadrilateral cells containing higher order hierarchical H(div) Legendre basis functions. The algorithm conveys an effective method for the numerically evaluation of the weak singular integrals. The results show that when the cell is changed from a rectangular to a quadrilateral shape the accuracy is essentially not affected, despite that the quadrilateral cell includes a sharp corner. This is of course only valid up to a certain degree, when the corner is not too sharp, but since the two shapes represent a straight line and a sharp corner it cover most of the common cases. The results also show that when the field point  $r = \{r_p : r_p \notin K_{uv}\}$  is close to the boundary of the cell, or the point  $r = \{r_p + \hat{n}d : r_p \in K_{uv}, d > 0\}$  is close to the quadrilateral surface the domain of integration includes regions of rapid variations which affects the accuracy of the integration. These points are stated as near-singular points. To overcome this problem the domain of integration is divided into several parts such that the quadrature points from the Gauss-Legendre algorithm are distributed in a more advantageous way. Points that are close to the boundary, but are not regarded as being near-singular, do not suffer from a slow convergence rate (see Figure 19 and Figure 20). Since the number of near-singular points are rather few the results convey that the influence on the accuracy is in most cases limited.

# References

- [1] M. G. Duffy. Quadrature over a pyramid or cube of integrands with a singularity at a vertex. SIAM Journal on Numerical Analysis, 19, 1260–1262, 1982.
- [2] J. Helsing. Integral equation methods for elliptic problems with boundary conditions of mixed type. *Journal of Computational Physics*, **228**(23), 8892–8907, 2009.
- [3] E. Jørgensen, J. L. Volakis, P. Meincke, and O. Breinbjerg. Higher-order hierarchical Legendre basis functions for iterative integral equation solvers with curvilinear surface modeling. *Proc. IEEE Antennas Propagation Society Int. Symp.*, 4, 618–621, June 2002.
- [4] M. A. Khayat and D. R. Wilton. Numerical evaluation of singular and near-singular potential integrals. *IEEE Trans. Antennas Propagat.*, **53**(10), 3180–3190, October 2005.
- [5] S. M. Rao, D. R. Wilton, and A. W. Glisson. Electromagnetic scattering by surfaces of arbitrary shape. *IEEE Trans. Antennas Propagat.*, **30**(3), 409–418, 1982.
- [6] G. Vecchi. Loop-Star Decomposition of Basis Functions in the Discretization of the EFIE. *IEEE Trans. Antennas Propagat.*, **47**(2), 339–346, February 1999.

[7] H. Xiao and Z. Gimbutus. A numerical algorithm for the construction of efficient quadrature rules in two and higher dimensions. *Comput. Math. Appl.*, **59**(2), 663–676, 2010.